25. http://dmtools.brown.edu
26. D. R. Tovey *et al.*, *Phys. Lett. B* **488**, 17 (2000).
27. F. Giuliani, *Phys. Rev. Lett.* **93**, 161301 (2004).
28. We gratefully acknowledge the effort and outstanding technical support of the Fermilab staff. This work is supported by NSF CAREER award PHY-0239812, NSF grants PHY-0707298 and PHY-0555472, the Indiana University South Bend R&D committee, the Kavli Institute for Cosmological Physics through grant NSF PHY-0114422, and the U.S. Department of Energy.

Supporting Online Material
www.sciencemag.org/cgi/content/full/319/5865/933/DC1

SOM Text
Figs. S1 to S3
References

31 August 2007; accepted 4 January 2008
10.1126/science.1149999

Electron-Driven Acid-Base Chemistry: Proton Transfer from Hydrogen Chloride to Ammonia

Soren N. Eustis,[1] Dunja Radisic,[1] Kit H. Bowen,[1]* Rafał A. Bachorz,[2,3] Maciej Haranczyk,[3,4] Gregory K. Schenter,[3] Maciej Gutowski[3,4,5]*

In contrast to widely familiar acid-base behavior in solution, single molecules of NH_3 and HCl do not react to form the ionic salt, $NH_4^+Cl^-$, in isolation. We applied anion photoelectron spectroscopy and ab initio theory to investigate the interaction of an excess electron with the hydrogen-bonded complex $NH_3 \cdots HCl$. Our results show that an excess electron induces this complex to form the ionic salt. We propose a mechanism that proceeds through a dipole-bound state to form the negative ion of ionic ammonium chloride, a species that can also be characterized as a deformed Rydberg radical, NH_4, polarized by a chloride anion, Cl^-.

When vapors from open bottles of concentrated hydrochloric acid and ammonium hydroxide intermingle, a white cloud consisting of tiny ammonium chloride particles forms. Yet for many years the question of how individual molecules of HCl and NH_3 interact ranked as a fundamental problem in acid-base chemistry. Essentially, two main types of interactions were posited: either a hydrogen-bonded, $ClH \cdots NH_3$ complex, or a proton-transferred (ionic) molecule, $NH_4^+Cl^-$, classified respectively by Mulliken as outer and inner complexes (*1*). Competition between covalent and ionic bonding, as well as the role of hydrogen bonding and proton transfer, made the HCl/NH_3 system a particularly attractive model for exploring the interplay between major concepts in chemistry. Eventually, the following question came into focus: Can a single molecule of NH_3 interacting with a single molecule of HCl undergo proton transfer to form $NH_4^+Cl^-$, or does the formation of such ionic species require the assistance of environmental, cooperative effects, like those found in the condensed phase?

For a time, the prevailing evidence leaned toward the proton-transferred outcome. In a series of experiments 20 years ago, however, Legon showed conclusively by rotational spectroscopy that in beams of neutral $[(HCl)(NH_3)]$ heterodimers (*2*, *3*), no appreciable proton transfer occurs; instead, the spectra are consistent with linear, hydrogen-bonded $ClH \cdots NH_3$ complexes. Modern theoretical studies agree (*4*–*11*). Therefore, as counterintuitive as it may seem, ammonia and hydrogen chloride do not react under isolated conditions. This finding also made it clear, however, that the appearance of the white clouds required outside interactions to induce proton transfer and thus salt formation. As a result, the answer to one question had raised another: Can local environmental effects, such as collisions with other molecules or interactions with electrons, ions, or even photons, trigger proton transfer in acid-base complexes such as these?

Here, we focus on a particular aspect of this general question: Can a single electron, the most fundamental entity in chemistry, cause the $ClH \cdots NH_3$ complex to undergo proton transfer to form an ionic salt? Although the synergy between electron and proton transfer is recognized as a fundamental process in biophysics, materials science, and catalysis (*12*, *13*), the detailed mechanisms responsible for many of these processes remain unresolved. The system under study can be viewed as undergoing a process quite similar to proton-coupled electron transfer (PCET). PCET reactions are commonly defined as those involving the concerted transfer of an electron and a proton in a given complex (*12*, *14*). However, there are variants of the PCET model that account for stepwise transfer (ET→PT, or PT→ET). These PCET reactions generally occur on nanosecond time scales, depending on the pathway and the overall driving force for the reaction. The present study is not time resolved, but the flight time of ions in our instrument ensures that all processes measured occur on a time scale less than ~100 μs.

Experimentally, we used anion photoelectron spectroscopy to study these species. Anion photoelectron spectroscopy is conducted by crossing a mass-selected beam of negative ions with a fixed-frequency photon beam and analyzing the energy of the resultant photodetached electrons. Photodetachment is a direct process that is governed by the energy-conserving relation, $h\nu$ = EBE + EKE, where $h\nu$ is the photon energy, EBE is the electron binding energy, and EKE is the electron kinetic energy. The known photon energy and measured electron kinetic energies yield the electron binding energies (anion-to-corresponding neutral transition energies). The anionic complexes of interest were generated in a nozzle-ion source. In this device, an ammonia/argon (15%/85%) mixture at 25°C and 2 atm was expanded through a 20-μm orifice into high vacuum, while a HCl/argon (10%/90%) mixture at a few Torr flowed from a small tube into the expansion region immediately outside the nozzle. Into this confluence of gases, low-energy electrons were injected from a biased filament nearby. This arrangement brought the three main components together in vacuum but very near the nozzle, where plentiful cooling collisions with argon atoms carried away the excess energy of the products. The nozzle and its stagnation chamber were biased at −500 V, and the entire region between the nozzle and the skimmer was subjected to a weak, axial magnetic field to enhance the stability of the microplasma. The resultant anions were then extracted and transported by a series of lenses through a 90° magnetic sector, which served as a mass analyzer and selector. By sweeping the magnet current and thus the magnetic field, anions were detected by a Faraday cup further downstream and a mass spectrum was thereby recorded. Ions of interest were then focused through an aperture and transported into the ion-laser interaction region, where they crossed a beam of ~200 W of 488-nm (2.540 eV) photons from an argon ion laser. Some of the resultant photodetached electrons then entered the optics of a hemispherical electron energy analyzer, where they were counted as a function of their electron kinetic energy. Our apparatus has been described in further detail elsewhere (*15*).

For the theoretical analysis, we used high-level, ab initio, quantum chemistry methods implemented with MOLPRO (*16*) and Gaussian03 (*17*) to characterize potential energy surfaces of the neutral and the anion. The potential energy surfaces were explored at the coupled cluster level

[1]Department of Chemistry, Johns Hopkins University, Baltimore, MD 21218, USA. [2]Center for Functional Nanostructures (CFN) and Institute of Physical Chemistry, Universität Karlsruhe (TH), D-76128 Karlsruhe, Germany. [3]Chemical and Materials Sciences Division, Pacific Northwest National Laboratory, Richland, WA 99352, USA. [4]Department of Chemistry, University of Gdańsk, 80-952 Gdańsk, Poland. [5]Department of Chemistry, Heriot-Watt University, EH14 4AS Edinburgh, UK.

*To whom correspondence should be addressed. E-mail: kbowen@jhu.edu (K.H.B.); m.gutowski@hw.ac.uk (M.G.)

of theory (*18*) with extended basis sets (*19*). The coupled cluster calculations included single and double excitations (CCSD) when producing potential energy maps and determining minimum energy structures, whereas additional perturbative triple excitations [CCSD(T)] were included when calculating the adiabatic electron affinity and vertical detachment energy (VDE). Two-dimensional (2D) potential energy surfaces were calculated for the neutral and the anion, with the geometrical variables being the H-Cl distance, which characterizes the extent of intermolecular proton transfer, and the N-Cl distance along which the low-frequency intermolecular stretching vibration occurs. The 2D vibrational problems were solved for the pseudo three-body system (Cl, H, NH_3) with the use of scaled skewed coordinates (*20*) and a discrete variable representation of the potentials (*21*), resulting in anharmonic energy levels for the neutral and the anion that take into account the coupling between the proton and dimer stretches. All vibrational modes were taken into account when calculating the Franck-Condon (FC) factors between the ground vibrational state of the anion and various energy states of the neutral. These calculations were performed in harmonic approximation, and molecular Hessians were determined at the second-order Møller-Plesset level of theory.

Because the dipole moment of the $ClH\cdots NH_3$ complex is known from Stark-effect measurements to be substantial (4.06 D) (*22*), one might predict the anionic complex to be dipole bound (*23*, *24*). However, the photoelectron spectrum of $[(NH_3)(HCl)]^-$ (Fig. 1A) differs drastically from the spectrum of $[(H_2O)(HCl)]^-$ (Fig. 1C), which is the water analog of the $[(NH_3)(HCl)]^-$ anionic complex and a genuine dipole-bound system (*25*). Because dipole-bound electrons interact weakly with their nuclear frameworks, their characteristic binding energies are typically very low. Moreover, for the same reason, there is little structural difference between dipole-bound anions and their neutral counterparts, which results in high FC overlap between the anion and its neutral counterpart during photodetachment and thus a single dominant peak in their photoelectron spectra. In this context, two observations make it clear that the photoelectron spectrum of $[(NH_3)(HCl)]^-$ is not that of a dipole-bound state. First, the well-developed set of vibrational features (FC profile) in the spectrum of $[(NH_3)(HCl)]^-$ is indicative of a notable structural difference between the anion and its corresponding neutral. Second, for the $[(NH_3)(HCl)]^-$ complex, the position of the maximum in the vibrational envelope corresponds to an EBE, which is an order of magnitude larger than that for the dipole-bound $[(H_2O)(HCl)]^-$ complex.

How, then, should we interpret the vibrational progression in the spectrum of the $[(NH_3)(HCl)]^-$ complex? More specifically, if the FC distribution of peak intensities is characteristic of potential energy surfaces of the neutral and the anion that differ appreciably along some geometrical degree of freedom, what is the nature of this degree of freedom? We hypothesize that excess electron attachment to the hydrogen-bonded $ClH\cdots NH_3$ complex is accompanied by intermolecular proton transfer, with the final product being $(NH_4^+Cl^-)^-$. Furthermore, $(NH_4^+Cl^-)^-$ can be characterized as $(NH_4)^0Cl^-$, where $(NH_4)^0$ is the ammonium Rydberg (neutral) radical. The ammonium Rydberg radical, NH_4^0, is a hydrogenic system in which an electron is bound to a closed-shell NH_4^+ cation core (*26*).

Our calculations support this hypothesis in revealing profound differences between the neutral and anionic potential surfaces (Figs. 2 and 3). Both systems have C_{3v} equilibrium structures, but the $N\cdots H\cdots Cl$ proton is coordinated to Cl in the neutral and to N in the anionic complex. Moreover, the Cl-N distance decreases by 0.249 Å from the neutral to the anion. Other geometrical degrees of freedom are much less affected (table S1). The calculated dipole moment of the $[(NH_3)(HCl)]$ system increases from 4.15 to 9.82 D upon the intermolecular proton transfer, indicative of the formation of the ionic pair, $(NH_4^+Cl^-)$. The binding of the excess electron by the cationic site and the formation of the $NH_4^0Cl^-$ radical anion are responsible for the very different peak profiles in the $[(H_2O)(HCl)]^-$ and $[(NH_3)(HCl)]^-$ spectra. Thus, the computational results predict that the qualitative differences

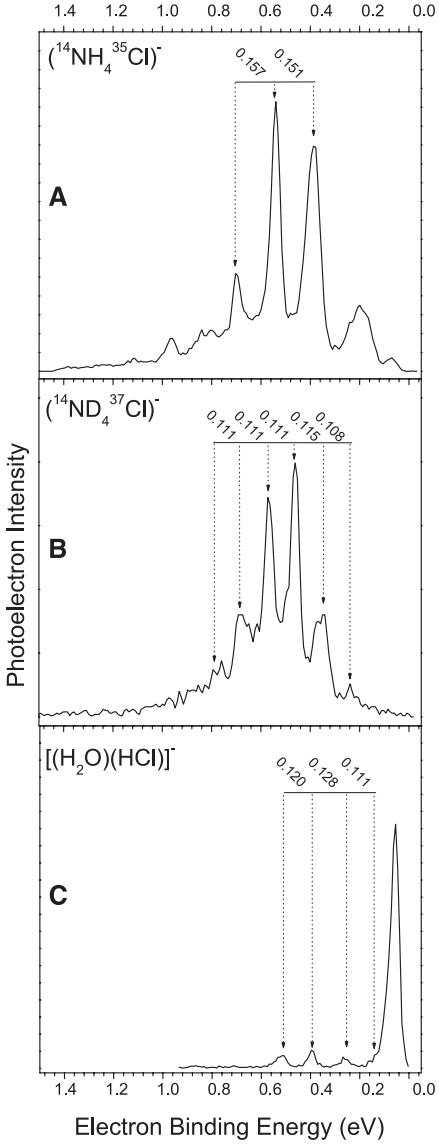

Fig. 1. Photoelectron spectra of (**A**) $(NH_4Cl)^-$, (**B**) $(ND_4Cl)^-$, and (**C**) the mixed dimer $[(H_2O)(HCl)]^-$. All spectra were recorded with 2.540-eV photons.

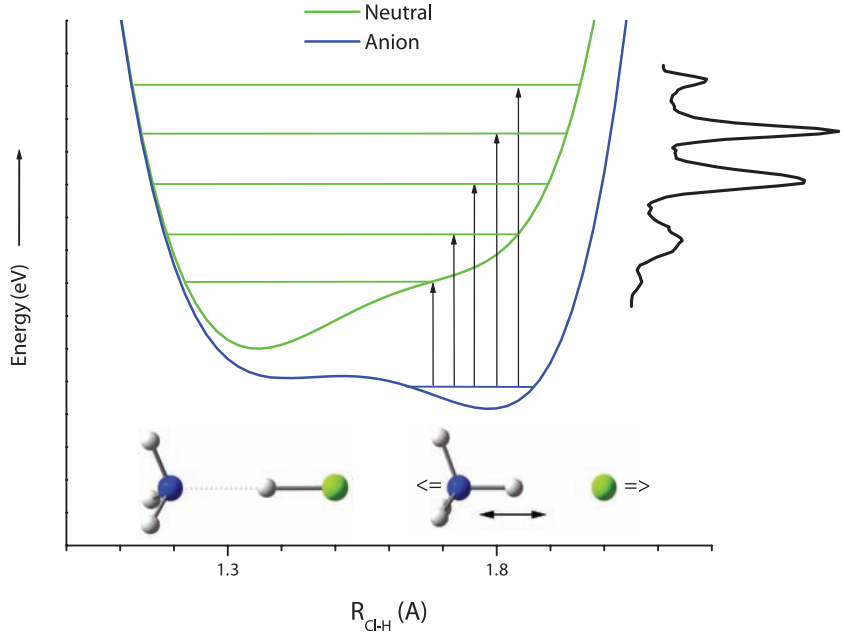

Fig. 2. One-dimensional potential energy curves for the neutral (upper) and anionic (lower) forms of $ClH\cdots NH_3$ and NH_4Cl. The two potential curves have been shifted in energy for clearer presentation. Figure 1A is presented alongside the neutral potential energy surface.

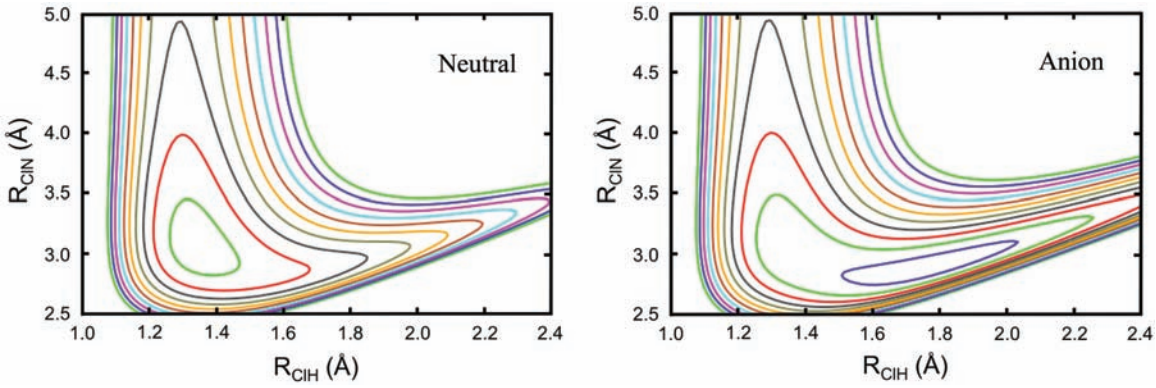

Fig. 3. Two-dimensional potential energy curves mapping the N-Cl and Cl-H bond lengths for the neutral (**left**) and anionic species (**right**). The contour line spacing is 0.005 Hartree.

in the photoelectron spectra of $[(H_2O)(HCl)]^-$ and $[(NH_3)(HCl)]^-$ result primarily from the intermolecular proton transfer from HCl to NH_3.

Quantitatively, the experimental and computational results are in excellent agreement. The EBE at the maximum of the most intense peak is 0.541 ± 0.010 eV, where the computed EBE value for the most prominent peak is predicted to be 0.512 eV. Essentially, these values are experimental and computational measures of VDE, the vertical detachment energy (the EBE of optimal FC overlap). Additionally, the transition between the lowest-energy vibrational level of the anionic state and the lowest-energy vibrational level of its neutral counterpart provides the value of the system's adiabatic electron affinity, and based on our spectral assignment, this value of 0.075 ± 0.020 eV agrees perfectly with the computed value of 0.075 eV.

How does the $ClH\cdots NH_3$ complex evolve, upon electron attachment, into the NH_4^0 Rydberg radical perturbed by Cl^-? As illustrated in Fig. 4, we envision a two-step process. Because the dipole moment of the neutral $ClH\cdots NH_3$ complex is easily big enough to trap an excess electron, the first step likely involves the formation of an incipient dipole-bound anionic complex. This is in contrast to our previous theoretical work on proton transfer in the formic acid dimer anion, in which the dipole moment is too low (1.74 D for the neutral monomer and zero for the dimer) to trap an electron (*27*). Our calculations show that the excess electron is held in an extremely diffuse cloud off the ammonia end of the $ClH\cdots NH_3$ complex and is vertically bound by only 0.03 eV (Fig. 4A). In the second step, this extra negative charge serves to facilitate the barrier-free transfer of the proton from HCl to NH_3, forming the $(NH_4^+Cl^-)^-$ anion (Fig. 4B). Thus, the dipole-bound anionic complex may be viewed as a stepping-stone to the more anionic salt $NH_4^0Cl^-$. In isolation, the NH_4^0 radical would be essentially spherical (Fig. 4C) with a calculated ionization potential (IP) of 5.08 eV, but in $NH_4^0Cl^-$, the unpaired electron is polarized and destabilized by the presence of the nearby Cl^- anion, and the electron binding energy decreases to 0.51 eV.

Our initial calculations revealed profound differences between the neutral and anionic potential surfaces for this system, and slices of these surfaces along the hydrogen-chlorine distance, $R_{Cl\text{-}H}$, are shown schematically in Fig. 2. The neutral surface exhibits a well that corresponds to the $ClH\cdots NH_3$ hydrogen-bonded complex, with no local minimum at the geometry of the neutral $NH_4^+Cl^-$ molecule. On the same distance scale, the corresponding anion surface exhibits a well at the geometry of $(NH_4^+Cl^-)^-$, and a ledge (without an associated local minimum) that corresponds to the hydrogen-bonded complex $(ClH\cdots NH_3)^-$. Thus, whereas the $(NH_4^+Cl^-)^-$ anion can exist as a stable entity in isolation, the neutral $NH_4^+Cl^-$ ionic molecule cannot, collapsing thermodynamically into a complex between intact molecules of NH_3 and HCl. Figure 2 also depicts the vertical photodetachment transitions from the potential well of the $(NH_4^+Cl^-)^-$ anion to the corresponding neutral potential surface. It is clear there is FC overlap, albeit small, between the $v = 0$ levels of the anion and neutral wells. Also, the most intense peaks in the experimental spectral profile can be assigned to transitions from the region near the center of the anion's well to the ledge portion of the neutral potential. These transitions correspond to highly excited vibrations within the greater anharmonic well of the neutral $NH_3\cdots HCl$ complex.

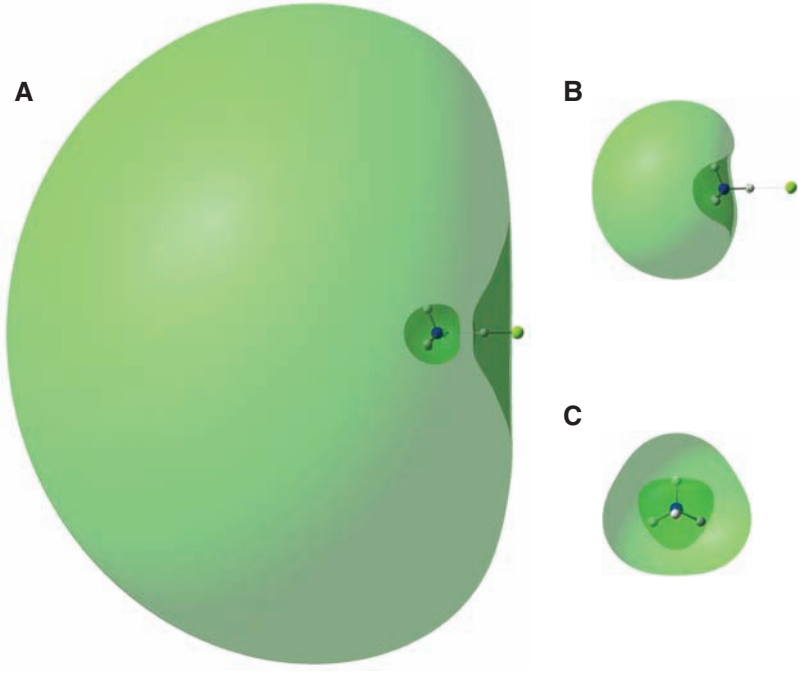

Fig. 4. Singly occupied molecular orbitals for (**A**) the dipole-bound intermediate $(ClH\cdots NH_3)^-$, (**B**) the proton-transferred species $(NH_4^+Cl^-)^-$, and for comparison (**C**) the neutral Rydberg radical (NH_4^0). Orbitals were generated with ChemCraft (*32*), and the resulting contours enclose 50% of the total excess electron density in each case. Calculated VDE values for (A) and (B) are 0.03 and 0.51 eV, respectively, and the calculated IP value for (C) is 5.08 eV.

The $(ND_4^+Cl^-)^-$ spectrum exhibits the same major progressions as does the $(NH_4^+Cl^-)^-$ spectrum, but with smaller energy spacings (Fig. 1, A and B). The most intense peaks show typical spacings of 0.154 eV (1242 cm^{-1}) in the $(NH_4^+Cl^-)^-$ spectrum and 0.111 eV (895 cm^{-1}) in the $(ND_4^+Cl^-)^-$ spectrum. The 1.387 ratio between the above spacings is quite close to $2^{1/2}$, the expected ratio for a H/D substitution in a hydrogen stretching mode. Infrared spectroscopic measurements of

NH_3/HCl and ND_3/DCl mixtures condensed in an argon matrix have been reported (*28*). Their spectra yield (v = 0→1) vibrational transition values of 1371 and 1113 cm^{-1}, respectively, for the N..H/D..Cl stretching modes of the proton-transferred species, $NH_4^+Cl^-$ and $ND_4^+Cl^-$. Because our spacings are extracted from highly anharmonic parts of the progressions and the (0→1) vibrational frequencies are strongly affected by matrix effects (*28*, *29*), the agreement is satisfactory. The first three calculated spacings between the energy levels associated with various excitations of the central hydrogen atom are 1718 (0 to 1), 1171 (1 to 2), and 1214 (2 to 3) cm^{-1}. The latter value of 1214 cm^{-1} matches very well the spacing between the two most prominent peaks [1218 cm^{-1} (0.151 eV)], suggesting that the two strongest peaks in the $(NH_4^+Cl^-)^-$ spectrum can be assigned as transitions from $v'' = 0$ in the anionic complex to $v' = 2$ and 3, respectively, in the neutral manifold (v'' denotes vibrational quantum numbers in the anion, v' signifies those in the neutral).

The secondary vibrational structure in the photoelectron spectra is likely associated with low-frequency vibrational modes, a prime candidate being the Cl-N intermolecular stretching mode. This is supported by the calculated decrease of the Cl-N distance by 0.249 Å from the neutral to the anion (Fig. 3). Both for the neutral and the anion, the theoretical calculations showed strong coupling between the central hydrogen and intermolecular stretching modes. (These two modes are schematically depicted in Fig. 2.) We calculated anharmonic spacings in the 155 to 172 cm^{-1} range (~0.02 eV) for the first five energy levels of the intermolecular stretching mode in the neutral complex.

These intermolecular stretching progressions are similar to those seen by Lineberger and coworkers (*30*) in their seminal work measuring the photoelectron spectra of the alkali halide anions. There are clear similarities between the current system, $NH_4{}^0Cl^-$, and the alkali halide anions, $(MX)^-$, which have also been described as M^0X^-. Their spectra, however, are dominated by the only available degree of freedom, the M-X stretch, whereas in the ammonia–hydrogen chloride system, transitions from that mode are far less prominent, with the N···H/D···Cl stretch giving rise to the dominant transitions.

References and Notes

1. R. S. Mulliken, W. B. Person, *Molecular Complexes, A Lecture and Reprint Volume* (Wiley-Interscience, New York, 1969).
2. N. W. Howard, A. C. Legon, *J. Chem. Phys.* **88**, 4694 (1988).
3. A. C. Legon, *Chem. Soc. Rev.* **22**, 153 (1993).
4. B. Cherng, F.-M. Tao, *J. Chem. Phys.* **114**, 1720 (2001).
5. F.-M. Tao, *J. Chem. Phys.* **110**, 11121 (1999).
6. R. Cazar, A. Jamka, F.-M. Tao, *Chem. Phys. Lett.* **287**, 549 (1998).
7. I. Alkorta, I. Rozas, O. Mo, M. Yanez, J. Elguero, *J. Phys. Chem. A* **105**, 7481 (2001).
8. A. Brciz, A. Karpfen, H. Lischka, P. Schuster, *Chem. Phys.* **89**, 337 (1984).
9. A. Famulari, M. Sironi, M. Raimondi, in *Quantum Systems in Chemistry and Physics* (Springer, Netherlands, 2000), vol. 1, pp. 361–379.
10. Z. Latajka, S. Sakai, K. Morokuma, H. Ratajczak, *Chem. Phys. Lett.* **110**, 464 (1984).
11. G. Corongiu *et al.*, *Int. J. Quant. Chem.* **59**, 119 (1996).
12. S. Y. Reece, J. M. Hodgkiss, J. Stubbe, D. G. Nocera, *Philos. Trans. R. Soc. B* **361**, 1351 (2006).
13. D. Radisic *et al.*, *J. Am. Chem. Soc.* **127**, 6443 (2005).
14. J.-Y. Fang, S. Hammes-Schiffer, *J. Chem. Phys.* **106**, 8442 (1997).
15. J. V. Coe, J. T. Snodgrass, C. B. Friedhoff, K. M. McHugh, K. H. Bowen, *J. Chem. Phys.* **87**, 4302 (1987).
16. MOLPRO, version 2006.1, a package of ab initio programs; H. J. Werner *et al.* (www.molpro.net).
17. Gaussian 03, Revision C.02; M. J. Frisch *et al.*, Gaussian, Inc., Wallingford CT, 2004.
18. P. R. Taylor, *Lecture Notes in Quantum Chemistry II*, B. O. Roos, Ed. (Springer-Verlag, Berlin, 1994).
19. We used augmented, polarized, correlation consistent basis sets of double- and triple-zeta quality (*31*) supplemented with additional diffuse s and p functions centered on the nitrogen atom with exponents chosen to describe the excess electron-charge distribution in the dipole-bound anion $(ClH\cdots NH_3)^-$.
20. B. C. Garrett, D. G. Truhlar, *J. Am. Chem. Soc.* **101**, 5207 (1979).
21. D. T. Colbert, W. H. Miller, *J. Chem. Phys.* **96**, 1982 (1992).
22. C. S. Brauer *et al.*, *J. Phys. Chem. A* **110**, 10025 (2006).
23. C. Desfrançois *et al.*, *Phys. Rev. Lett.* **72**, 48 (1994).
24. R. N. Compton *et al.*, *J. Chem. Phys.* **105**, 3472 (1996).
25. P. Skurski, M. Gutowski, *J. Chem. Phys.* **111**, 3004 (1999).
26. G. Herzberg, *Annu. Rev. Phys. Chem.* **38**, 27 (1987).
27. R. A. Bachorz, M. Haranczyk, I. Dabowska, J. Rak, M. Gutowski, *J. Chem. Phys.* **122**, 204304 (2005).
28. A. J. Barnes, T. R. Beech, Z. Mielke, *J. Chem. Soc. Faraday Trans. II* **80**, 455 (1984).
29. M. J. T. Jordan, J. E. Del Bene, *J. Am. Chem. Soc.* **122**, 2101 (2000).
30. T. M. Miller, D. G. Leopold, K. K. Murray, W. C. Lineberger, *J. Chem. Phys.* **85**, 2368 (1986).
31. R. A. Kendall, T. H. Dunning Jr., R. J. Harrison, *J. Chem. Phys.* **96**, 6796 (1992).
32. ChemCraft Version 1.5 (build 276), www.chemcraftprog.org.

33. This material is based in part on work supported by National Science Foundation grant CHE-0517337 (K.H.B.). We also thank the Polish State Committee for Scientific Research (KBN) for support under grants DS/8000-4-0026-8 (M.G.) and N204 127 31/2963 (M.H.) and the U.S. Department of Energy (DOE) Office of Basic Energy Sciences Chemical Sciences program (M.G. and G.K.S.). The research of R.A.B. was supported by the Deutsche Forschungsgemeinschaft (DFG) through the Center for Functional Nanostructures (CFN, Project No. C3.3) and by a grant from the Ministry of Science, Research and the Arts of Baden-Württemberg (Az: 7713.14-300). M.H. is a holder of an award from the Foundation for Polish Science (FNP). This research was performed in part at the Molecular Science Computing Facility in the William R. Wiley Environmental Molecular Sciences Laboratory at Pacific Northwest National Laboratory, operated for the U.S. DOE by Battelle.

Supporting Online Material

www.sciencemag.org/cgi/content/full/319/5865/936/DC1
Table S1

11 October 2007; accepted 21 December 2007
10.1126/science.1151614

High-Throughput Synthesis of Zeolitic Imidazolate Frameworks and Application to CO_2 Capture

Rahul Banerjee,[1]* Anh Phan,[1] Bo Wang,[1] Carolyn Knobler,[1] Hiroyasu Furukawa,[1] Michael O'Keeffe,[2] Omar M. Yaghi[1]*

A high-throughput protocol was developed for the synthesis of zeolitic imidazolate frameworks (ZIFs). Twenty-five different ZIF crystals were synthesized from only 9600 microreactions of either zinc(II)/cobalt(II) and imidazolate/imidazolate-type linkers. All of the ZIF structures have tetrahedral frameworks: 10 of which have two different links (heterolinks), 16 of which are previously unobserved compositions and structures, and 5 of which have topologies as yet unobserved in zeolites. Members of a selection of these ZIFs (termed ZIF-68, ZIF-69, and ZIF-70) have high thermal stability (up to 390°C) and chemical stability in refluxing organic and aqueous media. Their frameworks have high porosity (with surface areas up to 1970 square meters per gram), and they exhibit unusual selectivity for CO_2 capture from CO_2/CO mixtures and extraordinary capacity for storing CO_2: 1 liter of ZIF-69 can hold ~83 liters of CO_2 at 273 kelvin under ambient pressure.

High-throughput methods are routinely used in screening for activity of drug molecules and catalysts, but their use in the synthesis of new crystalline solid-state compounds remains relatively undeveloped. Often, the products are either known compounds or ones with condensed extended structures (*1*–*7*). For multicomponent chemical systems, such as in the synthesis of porous metal-organic structures, it would be reasonable to assume that the most energetically favored structures would result and that these would be known structures and topologies. Another challenge in solid-state synthesis is overcoming the propen-

[1]Center for Reticular Chemistry at California NanoSystems Institute, Department of Chemistry and Biochemistry, University of California at Los Angeles, 607 East Charles E. Young Drive, Los Angeles, CA 90095, USA. [2]Department of Chemistry and Biochemistry, Arizona State University, Tempe, AZ 85287, USA.

*To whom correspondence should be addressed. E-mail: rahul@chem.ucla.edu (R.B.); yaghi@chem.ucla.edu (O.M.Y.)